Continuous-wave operation of a frequency-tunable 460-GHz second-harmonic gyrotron for enhanced nuclear magnetic resonance

Continuous-Wave Operation of a Frequency-Tunable 460-GHz Second-Harmonic Gyrotron for Enhanced Nuclear Magnetic Resonance

Antonio C. Torrezan, *Student Member, IEEE*, Seong-Tae Han, Ivan Mastovsky, Michael A. Shapiro, Jagadishwar R. Sirigiri, *Member, IEEE*, Richard J. Temkin, *Fellow, IEEE*, Alexander B. Barnes, and Robert G. Griffin

***Abstract*—The design, operation, and characterization of a continuous-wave (CW) tunable second-harmonic 460-GHz gyrotron are reported. The gyrotron is intended to be used as a submillimeter-wave source for 700-MHz nuclear magnetic resonance experiments with sensitivity enhanced by dynamic nuclear polarization. The gyrotron operates in the whispering-gallery mode $TE_{11,2}$ and has generated 16 W of output power with a 13-kV 100-mA electron beam. The start oscillation current measured over a range of magnetic field values is in good agreement with theoretical start currents obtained from linear theory for successive high-order axial modes $TE_{11,2,q}$. The minimum start current is 27 mA. Power and frequency tuning measurements as a function of the electron cyclotron frequency have also been carried out. A smooth frequency tuning range of 1 GHz was obtained for the operating second-harmonic mode either by magnetic field tuning or beam voltage tuning. Long-term CW operation was evaluated during an uninterrupted period of 48 h, where the gyrotron output power and frequency were kept stable to within $\pm 0.7\%$ and ± 6 ppm, respectively, by a computerized control system. Proper operation of an internal quasi-optical mode converter implemented to transform the operating whispering-gallery mode to a Gaussian-like beam was also verified. Based on the images of the gyrotron output beam taken with a pyroelectric camera, the Gaussian-like mode content of the output beam was computed to be 92% with an ellipticity of 12%.**

***Index Terms*—Dynamic nuclear polarization (DNP), nuclear magnetic resonance (NMR), second cyclotron harmonic, submillimeter wave, terahertz, tunable gyrotron.**

Manuscript received September 20, 2009; revised March 2, 2010; accepted March 3, 2010. Date of publication April 22, 2010; date of current version June 9, 2010. This work was supported by the U.S. National Institutes of Health under Grant EB004866.

A. C. Torrezan is with the Department of Electrical Engineering and Computer Science and the Plasma Science and Fusion Center, Massachusetts Institute of Technology, Cambridge, MA 02139 USA (e-mail: torrezan@mit.edu).

S.-T. Han was with Plasma Science and Fusion Center, Massachusetts Institute of Technology, Cambridge, MA 02139 USA. He is now with the Korea Electrotechnology Research Institute, Ansan 426-170, Korea (e-mail: saiph@keri.re.kr).

I. Mastovsky, M. A. Shapiro, and J. R. Sirigiri are with Plasma Science and Fusion Center, Massachusetts Institute of Technology, Cambridge, MA 02139 USA (e-mail: ivan@psfc.mit.edu; shapiro@psfc.mit.edu; jags@mit.edu).

R. J. Temkin is with the Department of Physics and the Plasma Science and Fusion Center, Massachusetts Institute of Technology, Cambridge, MA 02139 USA (e-mail: temkin@mit.edu).

A. B. Barnes and R. G. Griffin are with the Department of Chemistry and the Francis Bitter Magnet Laboratory, Massachusetts Institute of Technology, Cambridge, MA 02139 USA (e-mail: barnesab@mit.edu; rgg@mit.edu).

Color versions of one or more of the figures in this paper are available online at http://ieeexplore.ieee.org.

Digital Object Identifier 10.1109/TPS.2010.2046617

I. Introduction

ONE of the scientific applications that have been driving the development of electromagnetic sources with moderate average power (tens of watts) in the millimeter- and submillimeter-wave bands is sensitivity-enhanced nuclear magnetic resonance (NMR) via dynamic nuclear polarization (DNP). In DNP/NMR, signal enhancement up to two orders of magnitude [1]–[3] can be obtained by transferring the high polarization of electron spins to nuclear spins through irradiation of a sample under study with electromagnetic waves at a frequency close to the electron Larmor frequency. In order to combine this signal enhancement technique with the improved spectral resolution and sensitivity provided by contemporary NMR spectrometers operating at magnetic fields greater than 5 T, microwave sources operating at frequencies higher than 140 GHz and able to deliver several watts to several tens of watts of output power are needed [1]. Long-pulse or continuous-wave (CW) operation with highly stable output power and frequency is also required from these sources in order to enable an efficient transfer of polarization [2] and long-term signal averaging in DNP experiments [3]. Another desirable feature that would advance DNP operation is smooth frequency tunability, where maximum signal enhancement could be obtained by tuning the microwave frequency instead of changing the NMR magnetic field. In addition, tunable sources would permit the implementation of DNP in current NMR spectrometers without the need for a sweep coil.

Among the submillimeter sources available to date, solid-state sources such as IMPATT and Gunn diodes have power capability limited to hundreds of milliwatts and tens of milliwatts at 140 GHz, respectively, dropping to a few milliwatts at 300 GHz [4]. A solid-state DNP source consisting of an oscillator connected to an amplifier and a chain of frequency multipliers is able to deliver a maximum output power of 33 mW at 264 GHz with a 3-dB frequency tuning range of 13.9 GHz [5]. Optically pumped far-infrared lasers can provide a series of discrete lines between 0.16 and 7.5 THz [6], with a maximum power of 1.2 W at 2.5 THz [7] reducing to a few milliwatts below 600 GHz in commercial versions [8], [9]. In the realm of vacuum electron devices, conventional tubes based on Cherenkov radiation utilize slow-wave structures with transverse dimensions on the order of the wavelength in order to provide waves with subluminal phase velocity to interact with

an electron beam. At high frequencies, these structures become more involved to fabricate and have limited average power capability. For example, even though commercially available extended-interaction oscillators are able to generate 25 W of power at 140 GHz at continuous duty, the output power of these devices reduces to 1 W at 220 GHz [10]. Backward-wave oscillators (BWOs), which have covered frequencies up to 1.4 THz, follow a similar trend with power dropping from about 10 W at 140 GHz to 1 W at 300 GHz [11].

On the other hand, fast-wave vacuum electron devices such as gyrotrons allow interaction between electrons and waves with superluminal phase velocity. These fast waves are supported by overmoded smooth waveguides, which are simpler to fabricate and able to handle the average power required for DNP/NMR and beyond. For instance, a gyrotron oscillator developed for fusion application has produced megawatt power levels at 170 GHz for a pulse length as long as 800 s [12]. Gyrotrons operating at the second harmonic of the electron cyclotron frequency have generated kilowatt power levels in the CW regime at 157, 250, and 326 GHz [13], [14].

Gyrotrons were first developed for high-field DNP/NMR at the Massachusetts Institute of Technology (MIT), Cambridge, USA, in the early 1990s initially at 140 GHz [15] and later at 250 GHz [16], corresponding to 211- and 380-MHz ^{1}H NMR frequencies, respectively. These gyrotrons operate at the fundamental harmonic of the cyclotron frequency and have generated 14 W at 140 GHz [17] and 7 W at 250 GHz [3] using low beam power (300 W) and low beam current (25 mA). Long-term continuous operation with stable output power and frequency has been demonstrated for both gyrotrons. In particular, the 250-GHz gyrotron has achieved uninterrupted and stable CW operation for a period of 21 days [3]. The possibilities and results [1]–[3], [15] provided by this new instrumentation have sparked the interest of other research laboratories [18]–[20] and companies [21] around the world, which are employing or developing gyrotrons for DNP/NMR spectrometers.

In order to extend the applicability of DNP/NMR to higher fields, the expensive cost of 10–22-T Nb_3Sn superconducting magnets can be avoided by operating the gyrotron at a cyclotron harmonic while utilizing less expensive NbTi superconducting magnets with fields up to 10 T. This option was first considered at MIT with the development of a second-harmonic 460-GHz gyrotron for a 700-MHz ^{1}H NMR system [22]. The first version of this gyrotron was able to generate up to 8.4 W of output power for a 12.4-kV 135-mA electron beam. The start current of the operating mode $TE_{0,6}$ was measured to be 67 mA, and stable continuous operation was demonstrated for a period of 1 h [23]. Another second-harmonic gyrotron was developed later at the University of Fukui, Fukui, Japan, for a 600-MHz DNP/NMR system [18]. Prospects to employ DNP to even higher NMR frequencies may be envisaged from a recent demonstration of 1-THz generation from a CW second-harmonic gyrotron [24].

A useful feature observed in the MIT 250- and 460-GHz gyrotrons was continuous frequency tunability due to the excitation of successive high-order axial modes as a function of magnetic field [3], [22]. While a tuning range broader than 2 GHz was observed for fundamental-harmonic modes, the continuous frequency tunability of second-harmonic modes was limited to a mere 50 MHz. Wideband magnetic tuning, which is similar to the tuning reported in [22], has recently been reported in a fundamental-harmonic 140-GHz gyrotron oscillator, with up to 6 GHz of magnetic tuning obtained [25]. For low-frequency gyrodevices operating at the second cyclotron harmonic, a smooth broadband magnetic tuning of 2.2 GHz has been observed in a 25-GHz CW gyro-BWO [26].

In this paper, we report the operational characteristics of a second-harmonic 460-GHz CW gyrotron. The tube was redesigned and rebuilt from a previous version for higher output power, lower start current, and improved stability/reliability. Broadband smooth frequency tunability was also obtained for the operating second-harmonic mode by changing the electron cyclotron frequency. This paper is organized as follows: Section II describes the design and features of the different parts of the tube, including the electron gun, the cavity interaction region, and the internal converter from a cylindrical waveguide mode to a linearly polarized free-space Gaussian-like beam. Evaluation of output power and frequency tunability as a function of magnetic field and beam voltage, start oscillation current of the operating mode, ohmic loss, frequency and power stability in long-run continuous operation, and output microwave beam profile is detailed in Section III. This paper is finalized with conclusions in Section IV.

II. Design

A schematic of the upgraded 460-GHz second-harmonic gyrotron is shown in Fig. 1, which shows the different parts of the tube: the electron gun, the cavity interaction region, the internal mode converter, and the collector.

A. Diode Electron Gun

The magnetron injection gun utilized in this work kept the same diode configuration and geometry of the previous version of the tube [22]. After being thermionically emitted from an indirectly heated ring cathode of radius 5.38 mm and slant length 1.09 mm, electrons are accelerated due to a potential difference between a grounded anode and a cathode at a beam voltage $-V_b$. As the electrons advance through the beam tunnel in cyclotron motion around the magnetic field lines created by the main superconducting magnet, the hollow annular electron beam is compressed, reaching a final beam radius of $r_b = 1.1$ mm in the cavity interaction region. The electron gun geometry is shown in Fig. 2(a), along with equipotential lines and electron trajectories obtained from the code EGUN [27] for the gyrotron operating parameters $V_b = 13$ kV and beam current $I_b = 100$ mA. Other important beam parameters, namely, the ratio of perpendicular to axial electron velocity known as the pitch factor α and the beam perpendicular velocity spread $\Delta v_\perp / v_\perp$, were also evaluated at the cavity region using EGUN. The results from these simulations are shown in Fig. 2(b), and a set of values favorable for beam–wave interaction, i.e., a high pitch factor ($\alpha \cong 2$) and a low perpendicular velocity spread ($\Delta v_\perp / v_\perp < 4\%$), was obtained at the operating voltage

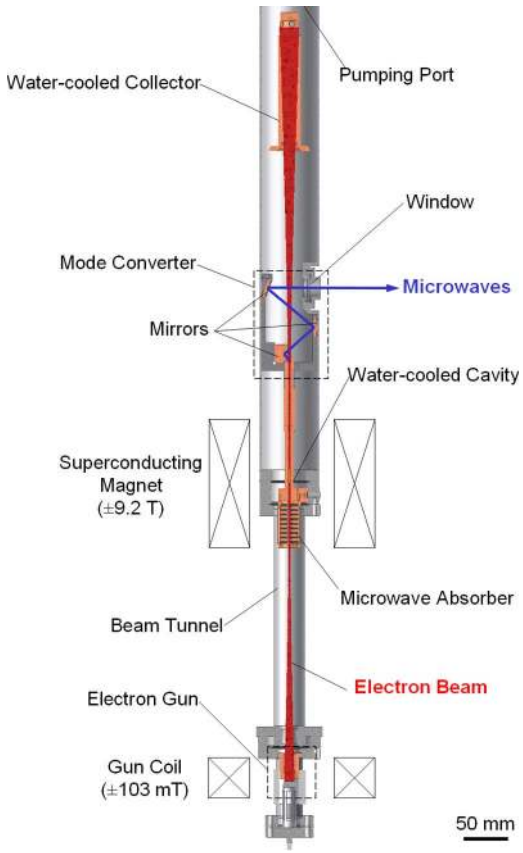

Fig. 1. Schematic of the 460-GHz gyrotron.

$V_b = 13$ kV by proper adjustment of a water-cooled copper gun coil with a magnetic field range of ± 103 mT.

B. Interaction Circuit

Although operation at the second harmonic of the cyclotron frequency has the advantage of requiring only half of the magnetic field necessary for a fundamental-harmonic mode, second-harmonic modes suffer from lower beam-wave interaction efficiency and from additional competition with neighboring fundamental modes. In order to overcome these difficulties, the $TE_{11,2}$ mode was chosen as the operating mode due to its isolation from surrounding modes and its high coupling to an electron beam of radius $r_b = 1.1$ mm. This whispering-gallery mode is supported by a 30-mm-long cylindrical cavity with radius $r_{\rm cav} = 1.825$ mm, where a long cavity (46λ at 460 GHz, where λ is the free-space wavelength) was preferred in order to reduce the start oscillation current. The interaction circuit geometry comprising a cavity straight section and tapered sections is shown in Fig. 3. The uptapered section was designed for reduced mode conversion and for reduced wave reflection at the cavity uptapered end to improve power extraction at the high operating frequency of the tube. The mode conversion in the uptapered part was found to be less than 0.2% according to calculations using the scattering matrix code Cascade [28]. Also shown in Fig. 3 is the normalized axial electric field profile of the first axial mode $TE_{11,2,1}$ obtained from a cold-cavity code [29].

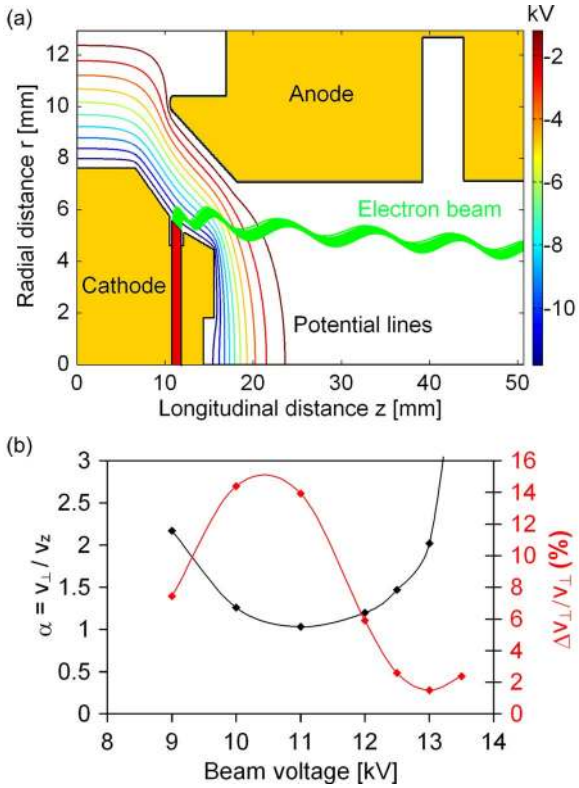

Fig. 2. (a) Magnetron injection gun geometry and simulated electron trajectories and equipotential lines for an applied voltage $V_b = 13$ kV and beam current $I_b = 100$ mA. (b) Computed pitch factor α and beam perpendicular velocity spread $\Delta v_\perp / v_\perp$ at the cavity entrance according to the code EGUN. The gun coil field was adjusted to a subtracting field of -61 mT for high α and low spread at the operating voltage 13 kV.

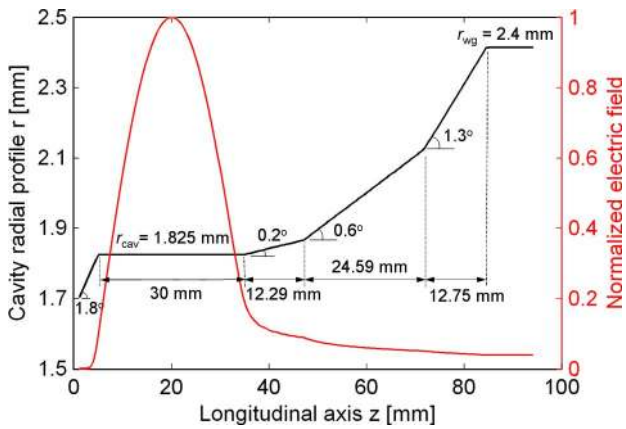

Fig. 3. Schematic of the 460-GHz gyrotron circuit featuring a downtaper section, a cavity (straight section), and an uptapered section. The red line represents the normalized axial electric field profile of the operating mode $TE_{11,2,1}$.

For the different axial modes $TE_{11,2,q}$, the ohmic quality factor was computed to be $Q_o = 8100$ for an electrical conductivity half that of ideal copper (5.8×10^7 S/m), and the diffractive quality factor was estimated as $Q_{D,q} = 90500/q^2$ according to the results from the cold-cavity code.

Based on linear theory [30] and the cold-cavity axial electric field profile, the start current of the $TE_{11,2,1}$ mode was computed to be 27 mA for beam parameters $V_b = 12.8$ kV, $\alpha = 1.85$, $r_b = 1.1$ mm, and no velocity spread. Following a similar

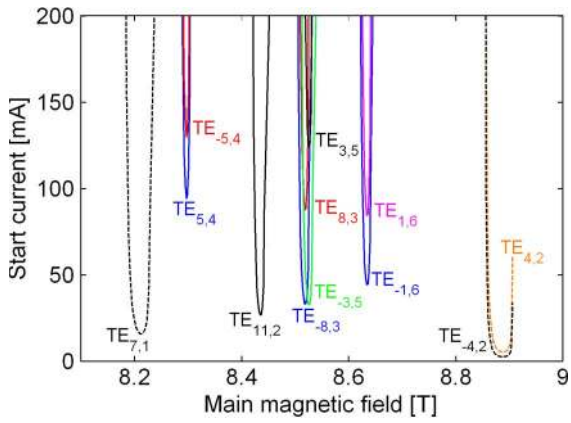

Fig. 4. Start oscillation current of cavity $\mathrm{TE}_{m,n,1}$ modes in the vicinity of the operating mode $\mathrm{TE}_{11,2,1}$. The dashed lines represent the fundamental-harmonic modes, while the solid ones refer to the second-harmonic modes. For each $\mathrm{TE}_{m,p,q}$ mode, only the lowest axial mode ($q = 1$) is shown (beam parameters: $V_b = 12.8$ kV, $r_b = 1.1$ mm, $\alpha = 1.85$, and no velocity spread).

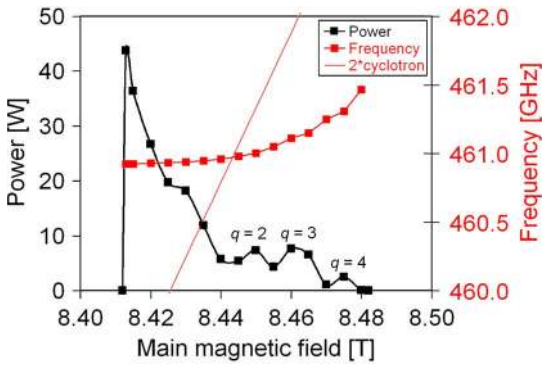

Fig. 5. Simulated power and frequency tuning as a function of magnetic field for the $\mathrm{TE}_{11,2}$ mode. Simulation parameters: $V_b = 13$ kV, $I_b = 100$ mA, $\alpha = 1.9$, $r_b = 1.1$ mm, $\Delta v_\perp / v_\perp = 5\%$, and $r_{\mathrm{cav}} = 1.822$ mm. In this simulation, the magnetic field profile was shifted 3.5 mm toward the cavity downtaper with respect to the cavity axial center.

procedure, the start current of the surrounding modes was also evaluated, and the result is shown in Fig. 4, which demonstrates the isolation of the operating second-harmonic mode from surrounding modes, particularly fundamental modes. The nomenclature $\mathrm{TE}_{m,p,q}$ denotes a cylindrical TE cavity mode with a radial mode number p, an axial mode number q, and an azimuthal mode number m, where a positive m refers to a mode corotating with respect to the electron gyration while a negative m refers to a counterrotating mode.

The performance of the interaction circuit was evaluated using the self-consistent code MAGY [31], and the simulation results are shown in Fig. 5 for beam parameters $V_b = 13$ kV, $I_b = 100$ mA, $\alpha = 1.9$, $r_b = 1.1$ mm, and a perpendicular velocity spread of 5%. A magnetic tuning range of 540 MHz was obtained supported by the excitation of successive axial modes $\mathrm{TE}_{11,2,q}$, $q = 1, 2, 3, 4$. The transition from the mode $\mathrm{TE}_{11,2,1}$ to $\mathrm{TE}_{11,2,2}$ was observed at a magnetic field value $B = 8.445$ T. Smoother transition in power between successive axial modes was verified in simulation by shifting the magnetic field profile 3.5 mm toward the cavity downtaper with respect to the cavity axial center.

The gyrotron cavity was manufactured by electroforming, where oxygen-free copper was deposited on an aluminum mandrel precisely machined to a tolerance of 2.5 μm in cavity diameter. After fabrication, the gyrotron cavity was cold tested, and the cavity radius was estimated to be 1.823 mm, corresponding to a cutoff frequency of 460.65 GHz for the $\mathrm{TE}_{11,2,1}$ mode. The cold test consisted of exciting lower order cavity modes such as $\mathrm{TE}_{0,1}$ and $\mathrm{TE}_{1,2}$ by means of a step-cut Vlasov converter and measuring the respective resonant frequencies using a vector network analyzer Agilent E8363B with a 90–140-GHz extension. Once the measured frequencies were corrected for a vacuum environment [32], the cold-cavity code was utilized to determine the cavity radius that would match the corrected frequency.

C. Internal Mode Converter and Collector

After transferring part of its perpendicular energy to the generated wave, the spent beam is separated from the electromagnetic wave by an internal mode converter, and it is allowed to expand in the decaying field of the superconducting magnet until it is collected on a water-cooled copper collector at ground potential. This internal mode converter configuration not only allows a reduction of the thermal load on the collector but also permits a better vacuum conductance throughout the tube, which contributes to the CW operation of the device. Meanwhile, a portion of the generated wave diffracts out of the resonator and propagates through the uptapered section followed by an output cylindrical waveguide of radius $r_{\mathrm{wg}} = 2.4$ mm. In the sequence, the cylindrical mode is internally converted into a linearly polarized free-space Gaussian-like beam, which is suitable for low-loss transmission to the NMR probe using a corrugated waveguide.

The internal mode converter is shown in Fig. 6(a) and consists of a helical launcher, a quasi-parabolic mirror, and two flat mirrors to deflect the microwave beam out of the tube through a transparent fused silica window of diameter 20.3 mm and thickness 2.00 mm, and a horizontal cross bore in the superconducting magnet. The converter design is based on a geometrical optics approach [33], [34], where the helical cut length was determined by

$$L_{\mathrm{CUT}} = 2\cot\theta_B r_{\mathrm{wg}} \sqrt{1 - \left(\frac{r_c}{r_{\mathrm{wg}}}\right)^2}\,\frac{\pi}{\theta} \tag{1}$$

where $\theta_B = \arcsin(k_\rho/k)$ is the Brillouin angle, $r_c = r_{\mathrm{wg}}(m/\nu'_{mp})$ is the caustic radius, and $\theta = \arccos(r_c/r_{\mathrm{wg}})$ is the azimuthal bounce angle. Here, k denotes the free-space wavenumber, and $k_\rho = \nu'_{mp}/r_{\mathrm{wg}}$ denotes the transverse wavenumber of the $\mathrm{TE}_{m,p,q}$ mode, where ν'_{mp} is the pth nonvanishing zero of the derivative of the Bessel function $J'_m(x)$. For the $\mathrm{TE}_{11,2}$ mode and output waveguide $r_{\mathrm{wg}} = 2.4$ mm, one has $L_{\mathrm{CUT}} = 11.2$ mm, $\theta_B = 49.5^\circ$, $r_c/r_{\mathrm{wg}} = 0.625$, and $\theta = 51.3^\circ$.

The design was evaluated using an electric field integral equation code Surf3d [35], and the computed electric field profile of the mode-converted $\mathrm{TE}_{11,2}$ output beam at 460 GHz is shown in Fig. 6(b). The simulated field profile has a Gaussian-like content of 92% with beam radii $w_x = 5.6$ mm and $w_y = 8.7$ mm at the window plane.

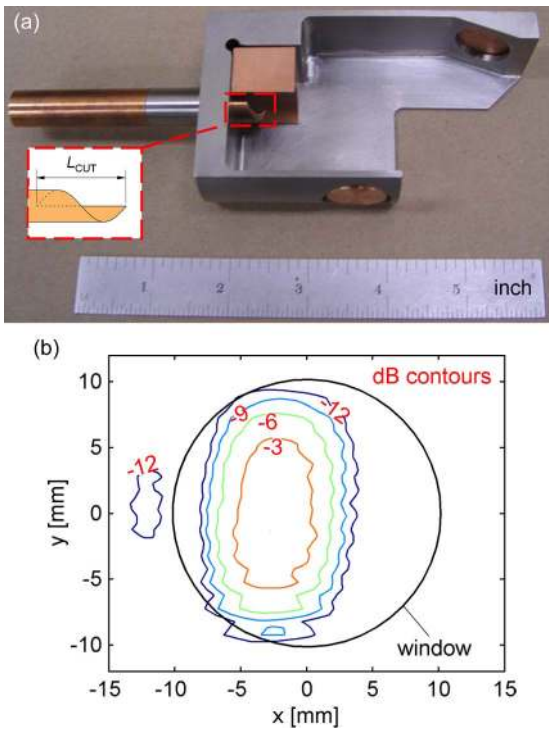

Fig. 6. (a) Quasi-optical mode converter picture with the inset showing the helical launcher orientation. (b) Simulated electric field profile of the mode-converted $TE_{11,2}$ output beam at the window plane at 460 GHz.

TABLE I
GYROTRON OPERATING PARAMETERS

Operating mode $TE_{m,p,q}$	$TE_{11,2,q}$
Frequency	460.2 GHz
Magnetic/voltage tuning range	1.0 GHz
Cavity magnetic field B	8.42 T
Cyclotron harmonic	Second
Beam voltage V_b	13 kV
Beam current I_b	100 mA
Output power	16 W (CW)

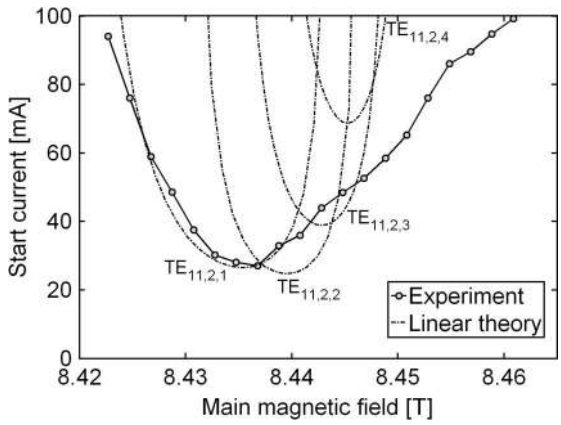

Fig. 7. (Solid line) Measured start oscillation current of the operating mode $TE_{11,2}$ as a function of magnetic field for beam voltage $V_b = 12.8$ kV and a gun coil field of -75 mT. Theoretical start currents based on linear theory for the first four axial modes $TE_{11,2,q}$, where $q = 1, 2, 3, 4$, are represented by dashed-dotted lines (simulation parameters: $r_{\rm cav} = 1.822$ mm, cold-cavity axial electric field profile, and beam parameters $V_b = 12.8$ kV and $\alpha = 1.85$, with no velocity spread).

III. EXPERIMENTAL RESULTS

The new version of the 460-GHz second-harmonic gyrotron was entirely processed and characterized in CW mode. The temperature of sensitive parts of the device, such as the anode, cavity, collector, and gun coil, was kept stable by a 2.4-kW recirculating chiller, with the water temperature and flow at each cooling channel being monitored by flowmeters. Relays existent in these flowmeters and in the ion pump controller formed a hardware safety interlock network ready to shut off the beam voltage if necessary. Software interlocks were also implemented in the computer control routine.

The output power was monitored at the end of a corrugated waveguide connected to the gyrotron window using, unless otherwise specified, a Scientech laser calorimeter model AC2500 calibrated for the submillimeter wavelength range. The corrugated waveguide employed in these measurements has an inner diameter of 19 mm and a corrugation depth of $\lambda/4$ [36]. The gyrotron frequency was measured using a heterodyne system, which consists of a harmonic mixer, an 18–26-GHz YIG-tuned local oscillator, a Phase Matrix 578B frequency counter utilized to monitor the local oscillator frequency, and an intermediate frequency section. The main gyrotron operating parameters are summarized in Table I.

A. Start Oscillation Current

The start oscillation current of the operating mode $TE_{11,2}$ was measured as a function of magnetic field for a fixed beam voltage $V_b = 12.8$ kV and a gun coil field of -75 mT. The result from this measurement is shown as a solid line in Fig. 7, and it is compared to theoretical start currents obtained from linear theory for the first four axial modes $TE_{11,2,q}$, where $q = 1, 2, 3, 4$. In these calculations, the axial electric field profile obtained from a cold-cavity code was employed, and the following beam parameters were assumed: $V_b = 12.8$ kV, $\alpha = 1.85$, and no velocity spread. The cavity radius was chosen to be $r_{\rm cav} = 1.822$ mm for best fit, which is within experimental error of the value (1.823 mm) obtained from the cavity cold test.

Good agreement between the measured and theoretical start currents for the first axial mode $TE_{11,2,1}$ is obtained at lower magnetic field values (< 8.44 T), where the minimum start current was measured to be 27 mA. This represents a start current much lower than 67 mA measured for the operating mode $TE_{0,6}$ in the previous version of the 460-GHz gyrotron [22]. The wider range of excitation of the measured start current compared to the magnetic field range of the theoretical start current for the $TE_{11,2,1}$ mode suggests that high-order axial modes ($q \geq 2$) are being observed in the experiment, which is in reasonable agreement with the calculated start currents for high-order axial modes $TE_{11,2,q}$, $q = 2, 3, 4$.

B. Power and Frequency Tuning

The 460-GHz gyrotron has generated 16 W of output power in the $TE_{11,2,1}$ second-harmonic mode for a 13-kV 100-mA electron beam, yielding an efficiency of 1.2%, a significant

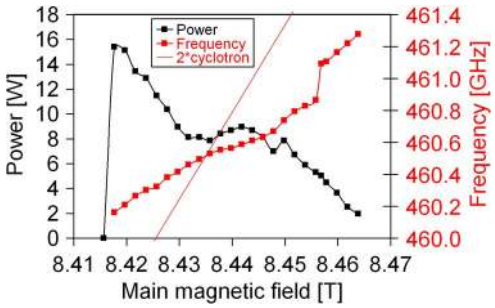

Fig. 8. Power and frequency tuning measurement as a function of magnetic field for the $TE_{11,2}$ mode, beam current $I_b = 100$ mA, and beam voltage $V_b = 13$ kV. The gun coil was swept from -75 to -78 mT for the best output power as the magnetic field was increased.

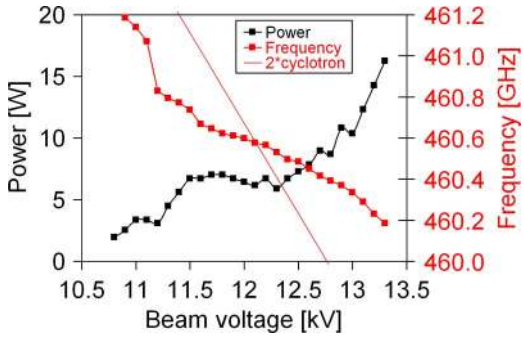

Fig. 9. Power and frequency tuning measurement as a function of beam voltage for the $TE_{11,2}$ mode, beam current $I_b = 100$ mA, and main magnetic field $B = 8.422$ T. The gun coil was swept from -71 to -103 mT for the best output power as the beam voltage was decreased from the maximum power point.

improvement compared to the 0.5% efficiency obtained in the previous configuration of this tube [23]. In addition, a smooth frequency tuning range of 1 GHz has been measured as a function of magnetic field for a constant 13-kV 100-mA electron beam, as shown in Fig. 8. This represents a tuning range 20 times broader than previously reported for a second-harmonic mode in a millimeter- and submillimeter-wave gyrotron. In the magnetic tuning measurement, the gyrotron output power was optimized by adjusting the subtracting gun coil field from -75 to -78 mT as the main magnetic field was increased, resulting in a minimum output power of 2 W throughout the tuning band.

The measured output power in Fig. 8 is in reasonable agreement with the self-consistent simulation result shown in Fig. 5, although more power was predicted in the simulation in the $TE_{11,2,1}$ mode at lower magnetic field values not accessible in the experiment.

As indicated by the start current measurement and the self-consistent simulations, the excitation of successive high-order axial modes $TE_{11,2,q}$ plays a role in providing the extended tuning as one increases the magnetic field for a fixed beam voltage. Electron beam interaction with backward-wave components of high-order axial modes is observed experimentally, and it occurs in a region where the gyrotron radiation frequency is less than the second harmonic of the electron cyclotron frequency. For the magnetic tuning measurement, the backward interaction region corresponds to magnetic field values greater than $B \cong 8.44$ T, a transition region from mode $TE_{11,2,1}$ to $TE_{11,2,2}$ as suggested by the start current measurement in Fig. 7 and the simulations in Fig. 5. Unlike in the simulation where the frequency tunability associated with the high-Q mode $TE_{11,2,1}$ was restricted to a few tens of megahertz, the measured tuning for the same mode reached a few hundreds of megahertz. One factor that may contribute to the broader tuning observed in the experiment is cavity thermal expansion due to the implemented cooling circuit covering a fraction of the cavity surface area.

Tuning measurements were also performed by changing the beam voltage while keeping the main magnetic field at $B = 8.422$ T and the beam current at $I_b = 100$ mA. The voltage tuning results are shown in Fig. 9, with similar output power and frequency tuning range compared to the magnetic tuning case. As the beam voltage was decreased from the maximum output power value, the gun coil had to be swept from -71 to -103 mT in order to keep a high α in the diode gun configuration for the best output power.

C. Ohmic Loss

At high-frequency operation, a significant part of the power transferred from the electron beam is not extracted from the gyrotron cavity, but instead, it is deposited in the cavity walls as ohmic loss. By measuring the water flow rate in the cavity cooling channel and the difference between its inlet and outlet temperature using thermistors, the amount of power transferred from the gyrotron cavity to the water cooling circuit could be calculated. For a gyrotron output power of 5.2 W at 460.28 GHz and a flow rate of 44 mL/s, the ohmic loss was estimated to be 53 W. Thus, only 9% of the power generated in the first axial mode $TE_{11,2,1}$ in the cavity is extracted as useful output power. This experimental extraction efficiency value η_{RF} is in good agreement with the theoretical one for the $TE_{11,2,1}$ mode, $\eta_{\mathrm{RF\_theory}} = (1 + Q_{D,1}/Q_o)^{-1} = 8\%$. The beam parameters during this measurement were $V_b = 12.9$ kV and $I_b = 79$ mA with the main magnetic field at $B = 8.423$ T.

D. CW Long-Term Stable Operation

Continuous gyrotron operation for extended periods with stable power and frequency characteristics is an important requirement to allow long-term signal averaging in DNP/NMR experiments. The long-term stability of the 460-GHz gyrotron operating in the $TE_{11,2}$ mode was evaluated for a period of two days, and the monitored variables are shown in Fig. 10. A quasi-optical directional coupler [37] was utilized at the end of the output corrugated waveguide to divert part of the output power to the frequency measurement system. The gyrotron output power was kept stable within $\pm 0.7\%$ by a computerized proportional, integral, and derivative (PID) control system implemented in LabVIEW that adjusted the cathode filament current based on the difference between a set point value and the output power monitored by a calibrated diode. This level of power fluctuation and the observed frequency stability of ± 2.9 MHz (± 6 ppm) are suitable for DNP/NMR. During the stability test, the main superconducting magnet was in persistent mode at $B = 8.422$ T, which has a magnetic field

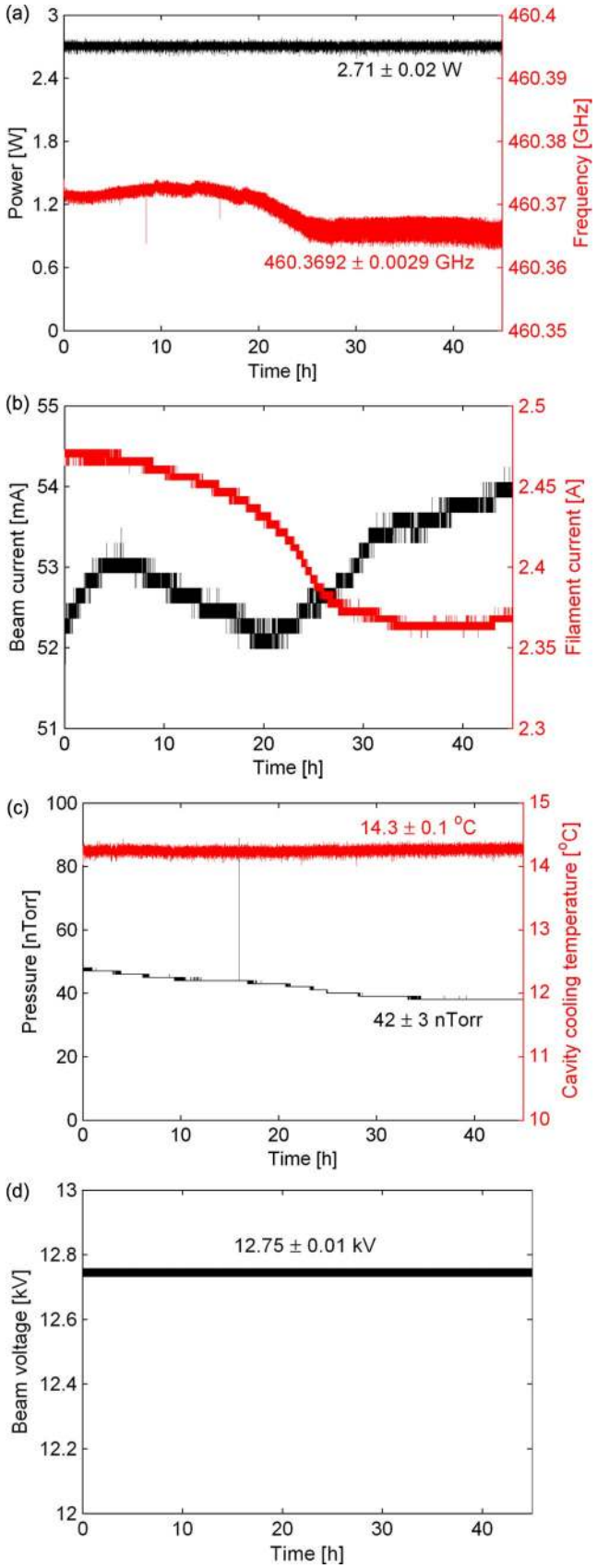

Fig. 10. Monitored variables during the long-term stability test of the 460-GHz gyrotron operating in the second-harmonic $TE_{11,2}$ mode: (a) output power and frequency, (b) beam and filament currents, (c) pressure and cavity cooling temperature, and (d) beam voltage. The main magnetic field was persistent at $B = 8.422$ T.

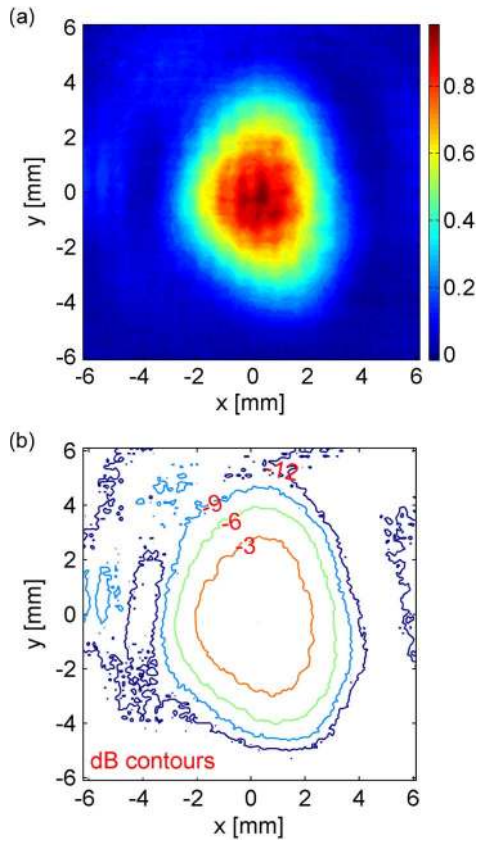

Fig. 11. Gyrotron output microwave beam displayed in (a) a normalized linear power scale and (b) decibel contours. The pyroelectric camera image of the mode-converted $TE_{11,2}$ mode at 460.3 GHz was taken 40 mm after the end of the corrugated waveguide.

drift rate of less than 0.02 ppm/h according to an NMR probe measurement.

E. Output Beam Pattern

The gyrotron output beam pattern was measured by a Spiricon Pyrocam III pyroelectric camera positioned after the corrugated waveguide connected to the gyrotron window. The camera consists of an array of 124-by-124 $LiTaO_3$ pyroelectric sensors with a spacing of 100 μm between each pixel, yielding an active area of 12.4 mm by 12.4 mm. Since the pyroelectric sensors are only sensitive to alternating signals, the CW microwave beam was modulated at a rate of 24 or 48 Hz by a built-in chopper located over the detection area. During the camera measurements, the gyrotron output power was limited to 0.4 W, below the camera sensor damage threshold of 2 W.

An image of the mode-converted $TE_{11,2}$ beam at 460.3 GHz captured 40 mm after the end of the corrugated waveguide is shown in Fig. 11. Based on the measured pattern, the Gaussian-like content associated with the measured microwave beam was computed to be 92% with beam radii $w_x = 4.1$ mm and $w_y = 4.6$ mm, corresponding to an ellipticity of 12%. Due to the limited access provided by the horizontal cross bore of the superconducting magnet, a direct beam measurement after the gyrotron window was not possible using the pyroelectric

camera. However, measurements performed with thermal paper inside the cross bore corroborated the camera results and confirmed the alignment of the output beam trajectory with respect to the cross bore centerline. These results indicate a good performance of the implemented internal quasi-optical converter from a whispering-gallery mode $TE_{11,2}$ to a Gaussian-like microwave beam at a submillimeter wavelength.

IV. Conclusion

The improved version of the 460-GHz second-harmonic gyrotron has generated 16 W of output power for a 13-kV 100-mA electron beam, yielding an efficiency of 1.2%. The minimum starting current of the operating mode $TE_{11,2,1}$ was measured to be 27 mA, agreeing with the linear theory prediction. Smooth frequency tunability of 1 GHz has been demonstrated for the operating second-harmonic mode as a function of the cyclotron frequency either by magnetic field tuning or beam voltage tuning. This frequency tuning range is 20 times broader than previously observed for a second-harmonic mode in a millimeter- and submillimeter-wave gyrotron. A frequency-tunable microwave source is highly desirable since it simplifies the implementation of DNP in NMR spectrometers, particularly the ones without sweep coils. The stability characteristics of the gyrotron have been evaluated during a period of two days in which the gyrotron operated continuously under computerized PID control monitoring the CW output power. A power stability of $\pm 0.7\%$ and a frequency stability of ± 2.9 MHz (± 6 ppm) have been obtained, which are suitable for the 700-MHz DNP/NMR application for which the gyrotron was designed. The Gaussian-like content of the measured mode-converted $TE_{11,2}$ output beam was calculated to be 92% with an ellipticity of 12%, indicating proper operation of the implemented internal quasi-optical mode converter.

Acknowledgment

The authors would like to thank J. Neilson for providing the code Surf3d.

References

[1] T. Maly, G. T. Debelouchina, V. S. Bajaj, K.-N. Hu, C.-G. Joo, M. L. Mak-Jurkauskas, J. R. Sirigiri, P. C. A. van der Wel, J. Herzfeld, R. J. Temkin, and R. G. Griffin, "Dynamic nuclear polarization at high magnetic fields," *J. Chem. Phys.*, vol. 128, no. 5, p. 052211, Feb. 2008.

[2] C.-G. Joo, K.-N. Hu, J. A. Bryant, and R. G. Griffin, "*In situ* temperature jump high-frequency dynamic nuclear polarization experiments: Enhanced sensitivity in liquid-state NMR spectroscopy," *J. Amer. Chem. Soc.*, vol. 128, no. 29, pp. 9428–9432, Jul. 2006.

[3] V. S. Bajaj, M. K. Hornstein, K. E. Kreischer, J. R. Sirigiri, P. P. Woskov, M. L. Mak-Jurkauskas, J. Herzfeld, R. J. Temkin, and R. G. Griffin, "250 GHz CW gyrotron oscillator for dynamic nuclear polarization in biological solid state NMR," *J. Magn. Reson.*, vol. 189, no. 2, pp. 251–279, Dec. 2007.

[4] R. J. Trew, "High-frequency solid-state electronic devices," *IEEE Trans. Electron Devices*, vol. 52, no. 5, pp. 638–649, May 2005.

[5] J. L. Hesler, D. S. Kurtz, Y. Duan, and T. W. Crowe, "Solid-state sources, receivers and systems for plasma diagnostics and THz frequency extenders for VNAs," in *Proc. IEEE 36th Int. Conf. Plasma Sci.*, San Diego, CA, Jun. 2009, p. 1.

[6] A. K. Hassan, L. A. Pardi, J. Krzystek, A. Sienkiewicz, P. Goy, M. Rohrer, and L.-C. Brunel, "Ultrawide band multifrequency high-field EMR technique: A methodology for increasing spectroscopic information," *J. Magn. Reson.*, vol. 142, no. 2, pp. 300–312, Feb. 2000.

[7] G. Dodel, "On the history of far-infrared (FIR) gas lasers: Thirty-five years of research and application," *Infrared Phys. Technol.*, vol. 40, no. 3, pp. 127–139, Jun. 1999.

[8] *THz Laser System*, Coherent, Inc., Santa Clara, CA, 2007. [Online]. Available: http://www.coherent.com/downloads/SIFIR50_DSrevB.pdf

[9] *Far Infrared Lasers*, Edinburgh Instruments, Livingston, U.K., 2010. [Online]. Available: http://www.edinst.com/fir.htm

[10] *Extended-Interaction Oscillators*, Commun. Power Ind. Inc., Palo Alto, CA, 2010. [Online]. Available: http://www.cpii.com/product.cfm/7/40/155

[11] G. Kantorowicz and P. Palluel, "Backward wave oscillators," in *Infrared and Millimeter Waves*, K. J. Button, Ed. New York: Academic, 1979, pp. 185–212.

[12] A. Kasugai, K. Sakamoto, K. Takahashi, K. Kajiwara, and N. Kobayashi, "Steady-state operation of 170 GHz–1 MW gyrotron for ITER," *Nucl. Fusion*, vol. 48, no. 5, p. 054009, May 2008.

[13] M. Thumm, "State-of-the art of high power gyro-devices and free electron masers, Update 2007," Forschungszentrum Karlsruhe, Karlsruhe, Germany, Sci. Rep. FZKA 7392, Mar. 2008.

[14] N. I. Zaytsev, T. B. Pankratova, M. I. Petelin, and V. A. Flyagin, "Millimeter- and submillimeter-wave gyrotrons," *Radio Eng. Electron. Phys.*, vol. 19, no. 5, pp. 103–107, May 1974.

[15] L. R. Becerra, G. J. Gerfen, R. J. Temkin, D. J. Singel, and R. G. Griffin, "Dynamic nuclear polarization with a cyclotron resonance maser at 5 T," *Phys. Rev. Lett.*, vol. 71, no. 21, pp. 3561–3564, Nov. 1993.

[16] K. Kreischer, C. Farrar, R. Griffin, R. Temkin, and J. Vieregg, "250 GHz gyrotron for NMR spectroscopy," in *Proc. IEEE 27th Int. Conf. Plasma Sci.*, New Orleans, LA, Jun. 2000, p. 198.

[17] C. D. Joye, R. G. Griffin, M. K. Hornstein, K.-N. Hu, K. E. Kreischer, M. Rosay, M. A. Shapiro, J. R. Sirigiri, R. J. Temkin, and P. P. Woskov, "Operational characteristics of a 14-W 140-GHz gyrotron for dynamic nuclear polarization," *IEEE Trans. Plasma Sci.*, vol. 34, no. 3, pp. 518–523, Jun. 2006.

[18] T. Idehara, I. Ogawa, L. Agusu, T. Kanemaki, S. Mitsudo, T. Saito, T. Fujiwara, and H. Takahashi, "Development of 394.6 GHz CW gyrotron (gyrotron FU CW II) for DNP/proton-NMR at 600 MHz," *Int. J. Infrared Millim. Waves*, vol. 28, no. 6, pp. 433–442, Jun. 2007.

[19] M. Silva, S. Alberti, J.-P. Ansermet, K. A. Avramides, G. Bodenhausen, J.-P. Hogge, I. Pagonakis, and D. Wagner, "Design of a low-power high-frequency gyrotron for DNP-enhanced NMR spectroscopy," in *Proc. IEEE 35th Int. Conf. Plasma Sci.*, Karlsruhe, Germany, Jun. 2008, p. 4 590 845.

[20] T. Idehara, L. Agusu, I. Ogawa, S. Kobayashi, T. Saito, R. Dupree, and M. E. Smith, "Development of gyrotron FU CW IIA for 600 MHz and 300 MHz DNP-NMR experiments at the University of Warwick," in *Proc. 33rd Int. Conf. Infrared, Millim. Terahertz Waves*, Pasadena, CA, Sep. 2008, pp. 1–2.

[21] Bruker Biospin, *263 GHz Solid State DNP-NMR Spectrometer*. [Online]. Available: http://www.bruker-biospin.com/dnp-dir.html

[22] M. K. Hornstein, V. S. Bajaj, R. G. Griffin, K. E. Kreischer, I. Mastovsky, M. A. Shapiro, J. R. Sirigiri, and R. J. Temkin, "Second harmonic operation at 460 GHz and broadband continuous frequency tuning of a gyrotron oscillator," *IEEE Trans. Electron Devices*, vol. 52, no. 5, pp. 798–807, May 2005.

[23] M. K. Hornstein, V. S. Bajaj, R. G. Griffin, and R. J. Temkin, "Continuous-wave operation of a 460-GHz second harmonic gyrotron oscillator," *IEEE Trans. Plasma Sci.*, vol. 34, no. 3, pp. 524–533, Jun. 2006.

[24] T. Idehara, I. Ogawa, H. Mori, S. Kobayashi, S. Mitsudo, and T. Saito, "A THz gyrotron FU CW III with a 20 T superconducting magnet," in *Proc. 33rd Int. Conf. Infrared, Millim. Terahertz Waves*, Pasadena, CA, Sep. 2008, pp. 1–2.

[25] T. H. Chang, T. Idehara, I. Ogawa, L. Agusu, and S. Kobayashi, "Frequency tunable gyrotron using backward-wave components," *J. Appl. Phys.*, vol. 105, no. 6, p. 063304, Mar. 2009.

[26] S. V. Samsonov, G. G. Denisov, V. L. Bratman, A. A. Bogdashov, M. Y. Glyavin, A. G. Luchinin, V. K. Lygin, and M. K. Thumm, "Frequency-tunable CW gyro-BWO with a helically rippled operating waveguide," *IEEE Trans. Plasma Sci.*, vol. 32, no. 3, pp. 884–889, Jun. 2004.

[27] W. B. Hermannsfeldt, "EGUN—An electron optics and gun design program," SLAC, Stanford, CA, Tech. Rep. SLAC-331 UC-28, Oct. 1988.

[28] *Cascade Engine v1.60*, Calabazas Creek Res., Inc., Saratoga, CA, 2001.

[29] A. W. Fliflet and M. E. Read, "Use of weakly irregular waveguide theory to calculate eigenfrequencies, Q values, and RF field functions

for gyrotron oscillators," *Int. J. Electron.*, vol. 51, no. 4, pp. 475–484, Oct. 1981.
[30] M. Yedulla, G. S. Nusinovich, and T. M. Antonsen, Jr., "Start currents in an overmoded gyrotron," *Phys. Plasmas*, vol. 10, no. 11, pp. 4513–4520, Nov. 2003.
[31] M. Botton, T. M. Antonsen, Jr., B. Levush, K. T. Nguyen, and A. N. Vlasov, "MAGY: A time-dependent code for simulation of slow and fast microwave sources," *IEEE Trans. Plasma Sci.*, vol. 26, no. 3, pp. 882–892, Jun. 1998.
[32] M. Blank, B. G. Danly, B. Levush, P. E. Latham, and D. E. Pershing, "Experimental demonstration of a W-band gyroklystron amplifier," *Phys. Rev. Lett.*, vol. 79, no. 22, pp. 4485–4488, Dec. 1997.
[33] S. N. Vlasov, L. I. Zagryadskaya, and M. I. Petelin, "Transformation of a whispering gallery mode propagating in a circular waveguide into a beam of waves," *Radio Eng. Electron. Phys.*, vol. 20, no. 10, pp. 14–17, Oct. 1975.
[34] E. M. Choi, M. A. Shapiro, J. R. Sirigiri, and R. J. Temkin, "Calculation of radiation from a helically cut waveguide for a gyrotron mode converter in the quasi-optical approximation," *J. Infrared Millim. Terahertz Waves*, vol. 30, no. 1, pp. 8–25, Jan. 2009.
[35] J. M. Neilson and R. Bunger, "Surface integral equation analysis of quasi-optical launcher," *IEEE Trans. Plasma Sci.*, vol. 30, no. 3, pp. 794–799, Jun. 2002.
[36] P. P. Woskov, M. K. Hornstein, R. J. Temkin, V. S. Bajaj, and R. G. Griffin, "Transmission lines for 250 and 460 GHz CW gyrotron DNP experiments," in *Proc. Joint 30th Int. Conf. Infrared Millim. Waves*, Williamsburg, VA, Sep. 2005, pp. 563–564.
[37] P. P. Woskov, V. S. Bajaj, M. K. Hornstein, R. J. Temkin, and R. G. Griffin, "Corrugated waveguide and directional coupler for CW 250-GHz gyrotron DNP experiments," *IEEE Trans. Microw. Theory Tech.*, vol. 53, no. 6, pp. 1863–1869, Jun. 2005.

Antonio C. Torrezan (S'04) received the B.S. and M.S. degrees in electrical engineering from the State University of Campinas (Unicamp), Campinas, Brazil, in 2004 and 2005, respectively. He is currently working toward the Ph.D. degree at the Massachusetts Institute of Technology (MIT), Cambridge.

From 2003 to 2005, he was with the Brazilian Synchrotron Light Laboratory (LNLS), where his research was focused on the development of an X-band EPR spectrometer for samples with small number of spins. In 2004, he was an Intern with the Brazilian Aeronautics Company (Embraer) in the area of control systems. Since 2005, he has been a Research Assistant with the Plasma Science and Fusion Center, MIT. His research interests include microwave and terahertz technologies, including submillimeter-wave sources such as gyrotrons.

Seong-Tae Han received the B.S. degree in physics education and the M.S. and Ph.D. degrees in physics from Seoul National University (SNU), Seoul, Korea, in 1999, 2001, and 2005, respectively.

As a Research Assistant, he participated in developing ultrawideband TWTs for electronic warfare and satellite communication at X-band. Moreover, he built the first working LIGA (deep-etched X-ray lithography and electroforming)-fabricated folded waveguide TWT operating at Ka-band. In 2005, he was a Researcher with the Research Institute of Basic Sciences, SNU, where his research focused on novel vacuum electron devices employing recent innovations, such as photonic crystal and cold cathode based on nano-/MEMS technologies. In September 2005, he joined the Plasma Science and Fusion Center, Massachusetts Institute of Technology, Cambridge, as a Postdoctoral Research Associate, where he worked on subterahertz gyrotrons (140 and 460 GHz) for DNP/NMR research and measurement of extremely low loss in the components of the 170-GHz ITER ECH transmission line. Since 2008, after completing his postdoctoral training, he has assumed a staff position with the Korea Electrotechnology Research Institute, Ansan, Korea. His research interest covers high-power subterahertz (0.1–1 THz) radiation sources and their applications in multidisciplinary convergence, as well as advanced vacuum electronics.

Ivan Mastovsky has been a Research Specialist with the Plasma Science and Fusion Center, Massachusetts Institute of Technology, Cambridge, for over 35 years. His research interests include free-electron lasers, relativistic magnetrons, high-power microwave tubes, and accelerators.

Michael A. Shapiro received the Ph.D. degree in radio physics from the University of Gorky, Gorky, Russia, in 1990.

Since 1995, he has been with the Plasma Science and Fusion Center, Massachusetts Institute of Technology, Cambridge, where he is currently the Head of the Gyrotron Research Group. His research interests include vacuum microwave electron devices, high-power gyrotrons, dynamic nuclear polarization spectroscopy, high-gradient linear accelerators, quasi-optical millimeter-wave components, and photonic bandgap structures and metamaterials.

Jagadishwar R. Sirigiri (S'98–M'03) received the B.Tech. degree in electronics engineering from the Institute of Technology, Banaras Hindu University, Varanasi, India, in 1996 and the S.M. and Ph.D. degrees in electrical engineering and computer science from the Massachusetts Institute of Technology (MIT), Cambridge, in 2000 and 2003, respectively.

From 1996 to 1998, he was a Senior Hardware Engineer with Wipro Infotech, India, where he was involved in the development of multimedia products, including hardware-based videoconferencing solutions. He demonstrated the first vacuum electron device with a photonic bandgap resonator to achieve single-mode operation in a highly overmoded device at 140 GHz. Since 2005, he has been a Research Scientist with the Plasma Science and Fusion Center, MIT, where he leads the experimental program in the Waves and Beams Division. His primary research areas include research and development of megawatt-class gyrotron systems for heating of fusion plasmas, millimeter- and submillimeter-wave gyrotrons for dynamic nuclear polarization in NMR experiments, slow- and fast-wave amplifiers in the W-band for radar and communication experiments, and high-gradient accelerators.

Dr. Sirigiri was the Guest Editor of the 12th Special Issue on High Power Microwaves of the IEEE TRANSACTIONS ON PLASMA SCIENCE in 2008.

Richard J. Temkin (M'87–SM'92–F'94) received the B.A. degree in physics from Harvard College, Harvard University, Cambridge, MA, and the Ph.D. degree in physics from the Massachusetts Institute of Technology (MIT), Cambridge.

From 1971 to 1974, he was a Postdoctoral Research Fellow with the Division of Engineering and Applied Physics, Harvard University. Since 1974, he has been with MIT, first with the Francis Bitter Magnet Laboratory and later with the Plasma Science and Fusion Center (PSFC) and the Department of Physics, where he is currently a Senior Scientist with the Department of Physics, the Associate Director of PSFC, and the Head of the Waves and Beams Division, PSFC. He has been the author or coauthor of over 200 published journal articles and book chapters and has been the Editor of six books and conference proceedings. His research interests include novel vacuum electron devices such as gyrotrons and free-electron lasers; advanced high-gradient electron accelerators; overmoded waveguides and antennas at millimeter/terahertz wavelengths; high-power microwave sources and their applications; plasma heating; and dynamic nuclear polarization/NMR.

Dr. Temkin is a Fellow of the American Physical Society and the Institute of Physics, London, U.K. He has been the recipient of the Kenneth J. Button Prize and Medal of the Institute of Physics, London, and the Robert L. Woods Award of the Department of Defense for Excellence in Vacuum Electronics research.

Alexander B. Barnes received the B.A. degree in chemistry from Whitman College, Walla Walla, WA, in 2003. He is currently working toward the Ph.D. degree in physical chemistry at the Massachusetts Institute of Technology (MIT), Cambridge.

Since 2004, he has been a Research Assistant with the Francis Bitter Magnet Laboratory, MIT, where he is developing dynamic-nuclear-polarization-enhanced solid-state nuclear magnetic resonance as a structure determination technique for membrane proteins and other biomolecules.

Robert G. Griffin received the B.S. degree in chemistry from the University of Arkansas, Fayetteville, in 1964 and the Ph.D. degree in physical chemistry from Washington University, St. Louis, MO, in 1969. He did his postdoctoral research in physical chemistry at the Massachusetts Institute of Technology (MIT), Cambridge, with Prof. J. S. Waugh.

In 1972, after completing his postdoctoral training, he assumed a staff position with the Francis Bitter Magnet Laboratory (FBML), MIT. In 1984, he was promoted to Senior Research Scientist. In 1989, he was appointed to the faculty with the Department of Chemistry, MIT. In 1992, he became the Director of FBML and is concurrently the Director of the Harvard Center for Magnetic Resonance, MIT, where he has been the Associate Director since 1989. He has published more than 300 articles concerned with magnetic resonance methodology and applications of magnetic resonance (NMR and EPR) to studies of the structure and function of a variety of chemical, physical, and biological systems. In the last decade, his research has focused on the development of methods to perform structural studies of membrane and amyloid proteins and on the utilization of high-frequency (> 100 GHz) microwaves in EPR experiments and in the development of dynamic nuclear polarization/NMR experiments at these frequencies. He has served on numerous advisory and review panels for the National Science Foundation and the National Institutes of Health.